Adsorption and Diffusion of Light Hydrocarbons in UiO-66(Zr): A Combination of Experimental and Modeling Tools

ARTICLE *in* THE JOURNAL OF PHYSICAL CHEMISTRY C · OCTOBER 2014

Impact Factor: 4.77 · DOI: 10.1021/jp509672c

11 AUTHORS, INCLUDING:

Philip L Llewellyn
Aix-Marseille Université
241 PUBLICATIONS **8,376** CITATIONS
SEE PROFILE

Vincent Guillerm
Autonomous University of Barcelona
37 PUBLICATIONS **1,455** CITATIONS
SEE PROFILE

Christian Serre
Université de Versailles Saint-Quentin
323 PUBLICATIONS **22,716** CITATIONS
SEE PROFILE

Guillaume Maurin
Université de Montpellier
218 PUBLICATIONS **6,814** CITATIONS
SEE PROFILE

THE JOURNAL OF PHYSICAL CHEMISTRY C

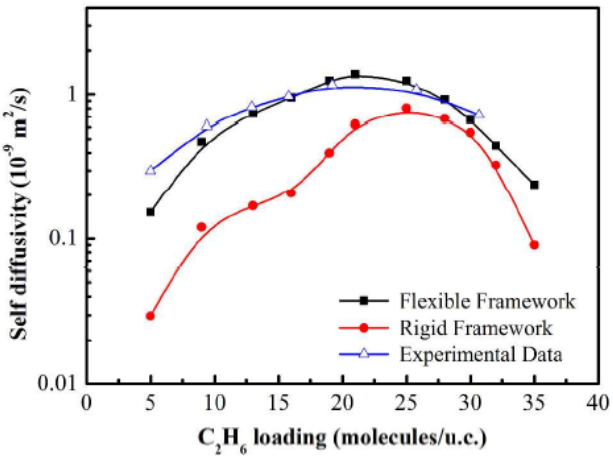

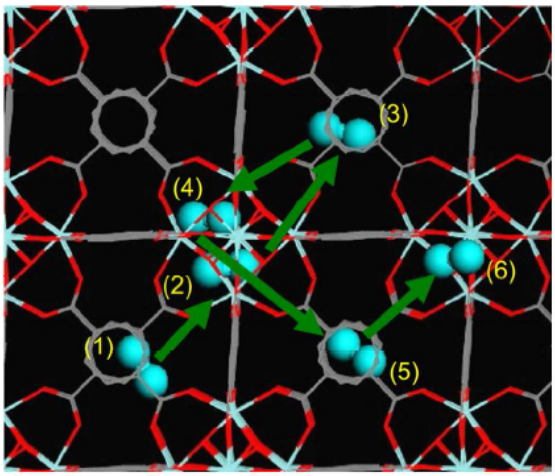

Adsorption and Diffusion of Light Hydrocarbons inUiO-66(Zr): A Combination of Experimental and Modelling Tools

THE JOURNAL OF PHYSICAL CHEMISTRY C

Article

pubs.acs.org/JPCC

Adsorption and Diffusion of Light Hydrocarbons in UiO-66(Zr): A Combination of Experimental and Modeling Tools

N. A. Ramsahye,*[,†,‡] J. Gao,[§] H. Jobic,[∥] P. L. Llewellyn,[⊥] Q. Yang,*[,§] A. D. Wiersum,[⊥] M. M. Koza,[#] V. Guillerm,[¶] C. Serre,[¶] C. L. Zhong,[§] and G. Maurin[†,‡]

[†]Institut Charles Gerhardt Montpellier, UMR CNRS 5253 UM2 ENSCM UM1, ENSCM, 8 rue de l'Ecole Normale, 34296 Montpellier Cedex 05, France

[‡]Institut Charles Gerhardt Montpellier, Université Montpellier 2, Place E. Bataillon, 34095 Montpellier Cedex 05, France

[§]Department of Chemical Engineering, Beijing University of Chemical Technology, Beijing 100029, China

[∥]Institut de Recherches sur la Catalyse et l'Environnement de Lyon, CNRS, Université de Lyon, 2. Av. A. Einstein, 69626 Villeurbanne, France

[⊥]Aix-Marseille Université, CNRS, Laboratoire MADIREL (UMR7246), Centre de Saint Jérôme, 13397 Marseille Cedex 20, France

[#]Institut Laue Langevin, BP 156, 39042 Grenoble, France

[¶]Institut Lavoisier, UMR CNRS 8180−Université de Versailles St Quentin en Yvelines, 45 avenue des Etats-Unis, Versailles 78035, France

Supporting Information

ABSTRACT: The concentration dependence of the self-diffusivity of short-chain linear alkanes in the narrow window type metal−organic framework (MOF) UiO-66(Zr) has been studied by means of quasi-elastic neutron scattering (QENS) measurements combined with molecular dynamics (MD) simulations. These computations employ a force field to describe the host/guest interactions which was preliminarily validated on the adsorption data obtained for the system of interest via gravimetry and microcalorimetry measurements. The QENS-measured self-diffusivity profile presents a non-monotonic tendency as the alkane loading increases, with the existence of a maximum that depends on the size of the alkane. The comparison with the simulated results obtained using either a flexible or a rigid framework highlights that the consideration of the flexibility is of prime importance when exploring the diffusion of ethane molecules in porous materials. The self-diffusivities subsequently calculated for propane and *n*-butane corroborate the results obtained for ethane, leading to a similar form for the plots of self-diffusion coefficient vs loading. The global microscopic diffusion mechanism is further shown to involve a combination of intracage motions and jump sequences between the tetrahedral and octahedral cages of the framework. The self-diffusion coefficients which decrease with increasing molecular size, and thus increasing confinement, are further compared to the values previously reported for MOFs with pore networks of different dimensions.

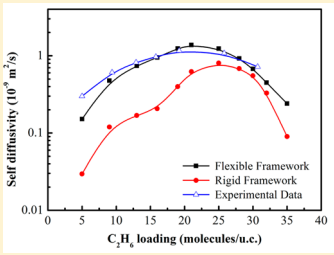

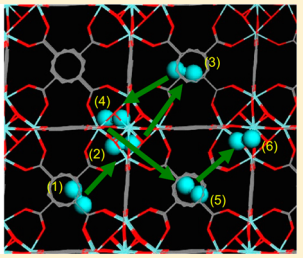

INTRODUCTION

Efficient gas storage and separation processes are of paramount importance in the chemical industry. For example, natural gas is made up of several hydrocarbon components including short-length alkanes, and their separation is of importance from the point of view of purification for energy applications.[1−5] Currently, this is achieved principally by means of physisorption-based processes involving the use of efficient adsorbents such as zeolites[6] and, to a lesser extent, pillared layered clays and porous carbons.[7] While such a separation is mainly driven by thermodynamic considerations, the diffusive properties of gases confined in these kinds of porous media can also play a significant role, and an exploration of this topic is an important step for the improvement of potential adsorbents. The delivery process of methane from natural gas can also be affected by the presence of low amounts of other short-length alkanes including ethane, propane, and *n*-butane. This calls for a deeper understanding of the diffusion mechanism for this series of species within the pores of the adsorbents.

Studies of diffusion of hydrocarbons in zeolites are abundant in the literature, detailed with both experimental and computational approaches. Some examples of work on short-chain hydrocarbons include the contribution of Demontis and Suffritti who explored the diffusion of methane and ethane in different zeolites (ZK4, NaA, silicalite, $AlPO_4$-5) using molecular dynamics (MD) simulations.[8−11] This computational

Received: September 24, 2014
Revised: October 28, 2014

dx.doi.org/10.1021/jp509672c | J. Phys. Chem. C XXXX, XXX, XXX−XXX

approach was also intensively employed by Smit and co-workers to predict the diffusion of short-length linear alkanes in a series of zeolites.[12−15] Krishna et al.[16] investigated the Maxwell−Stefan (M−S) and self-diffusivities of methane, ethane and propane in a variety of zeolites including MFI, ISV, BEA, AFI, FER, FAU, and LTA, at different loadings by means of MD simulations, as well as propane, *n*-butane and other alkanes in diverse materials such as cobalt formate frameworks.[17] Yashonath et al.,[18] Sayeed et al.,[19] and Snurr et al.[20] looked at the diffusion of methane and propane, respectively, in NaY. Molecular simulations have also been used to study gas mixtures. Examples include the work of Maurin et al.[21] and Snurr et al.,[22] who explored the diffusion of CH_4 in the presence of CO_2 (Maurin), and CH_4, C_3H_8, and *n*-C_4H_{10} in the presence of CF_4 (Snurr) in NaY. Maurin et al. also looked at the dynamics of a CH_4/CO_2 mixture in $AlPO_4$-5.[23] Hussain and Titiloye[24] concentrated on silicalite, studying the diffusion of pure and mixed alkanes by MD simulations. The concentration dependence of the self-diffusivity of ethane and ethylene in NaA zeolite was simulated by Gladden et al.[25] using Monte Carlo lattice dynamics, while Dubbeldam et al.[26] used a transition state theory approach to explore the diffusion of methane, ethane, and propane in LTA and LTL zeolites.

On the experimental side, a series of techniques including pulsed-field gradient (PFG) NMR, quasi-elastic neutron scattering (QENS),[27] and interference microscopy[28] have been widely employed to characterize the self-diffusivity of short-length linear alkanes in different zeolites. The main contribution emanates from Jobic,[29−36] Kaerger,[37−39] and co-workers who explored diffusion phenomena in diverse zeolites including MFI, silicalite, NaY, NaX, ZSM-5, and $AlPO_4$-5. The use of QENS for the measurement of the alkane diffusion has also been extended to a study of sol−gel derived silica.[40] Binder et al.[28] have illustrated the use of interference microscopy for the exploration of the intracrystalline diffusion of small hydrocarbons in DDR zeolites. Dai et al.[41] performed pulsed-field gradient (PFG) NMR experiments to study the self-diffusivities of ethane and ethylene in large-crystalline SAPO-34. The works of Caro et al.[42] and Hedin et al.[43] serve as further examples of the use of PFG NMR for the study of alkane diffusion in zeolites. However, although zeolites are widely used in industry for such separation tasks, they present a number of shortcomings, including an expensive high-temperature regeneration step, meaning that more energy-efficient materials would improve this process.

Metal−organic frameworks (MOFs) are potential storage and separation materials for a range of different gases including CO_2, H_2, N_2, and CH_4, as well as short- and long-chain hydrocarbons.[1,44−50] These porous hybrid materials have several interesting features such as large adsorption capacity and shape/size channel adjustability with respect to traditional porous materials, including the aforementioned zeolites and different types of carbons.[1,3,4,45,49,51,52] Additionally, we can further regulate and control the adsorption/separation abilities of this relatively new class of these solids by changing the nature of the organic linkers which interconnect the inorganic moieties to form the porous network.[53] Therefore, via such a chemical modification, the interactions between the porous materials and the guest molecules can be tuned to the required level. Several studies using a variety of experimental and computational techniques have already been published on the diffusion of short-length linear hydrocarbons in MOFs, either as pure phases or in the context of a mixture, for example, ethane and ethene. Chmelik et al.[54] investigated the intracrystalline diffusion of alkanes (including ethane and *n*-butane) in HKUST-1 and ethane in ZIF-8, using infrared microscopy (IRM), the same technique used in a study of ethane in ZIF-8 by the same group.[55] HKUST-1 was also the subject of the work of Wehring et al.,[56] where PFG NMR was combined with MD simulations to examine the diffusivity of the series of alkanes from propane to *n*-hexane. PFG NMR was also deployed by Stallmach et al.[57] to measure the self-diffusion coefficients of several alkanes in MOF-5, as well as by Chmelik et al.,[58] who evidenced a favorable diffusion selectivity for ZIF-8 toward ethene in an ethene/ethane mixture. The dynamics of methane in different MOFs was probed via MD calculations by Skoulidas et al.[59] Such a computational strategy was also deployed by Seehamart et al.[60,61] to explore the self-diffusivity of ethane in the MOF Zn(tbip) (H_2tbip = 5-*tert*-butyl-isophthalate acid), as well as a methane/ethane mixture in the same MOF,[62] followed by the works reported by Babarao et al.[63] and Krishna et al.[64] on the diffusion of different short-length hydrocarbon isomers in PCN-6 among others.

QENS measurements were also coupled with MD simulations to characterize the diffusion of small molecules and hydrocarbons in a series of MOFs including MIL-47(V)/MIL-53(Cr),[48,65−71] ZIF-8,[72] and UiO-66(Zr).[50,73,74]

The pore systems of certain MOFs (such as MIL-47(V)) are composed of channels where the molecular diffusion can take place relatively unhindered in one dimension.[71] However, motion in three dimensions can also be envisaged in certain other frameworks showing appropriate pore topology, for example, IRMOF-1, which has a channel system in all three directions. Another type of framework topology consists of cages of different sizes interconnected via windows, in which an adsorbate would have to exclusively migrate between cages, with no possibility of diffusion in a pore channel. A prominent example of such a MOF system is UiO-66(Zr) (UiO stands for University of Oslo).[75] This MOF is built up from $Zr_6O_6(CO_2)_{12}$ units interlinked via terephthalate linkers, forming a pore system with two types of cages of different sizes (free diameters of ca. 8 and 11 Å for the tetrahedral and octahedral cages, respectively), which are joined together through triangular windows (see Figure 1). The diffusion mechanism of a small molecule in such a MOF is more complex than that seen for MOFs with one-dimensional channels, such as MIL-47(V), since it is necessary for a guest molecule to enter and exit the different cages via the interconnecting windows, and these steps would have an associated energy barrier to overcome.[73,74] Indeed, UiO-66(Zr) may be considered as a model system for this kind of pore topology, and since the material has been shown to possess a high thermal and mechanical stability, as well as a good resistance to different solvents, with a well-controlled synthesis procedure,[76,77] it is a promising candidate for further application in the field of adsorption and separation.[50,78−80]

While this Zr-based MOF has been the subject of several adsorption studies,[77,78,81−93] the literature on the diffusion of confined molecules within its pores is still scarce. Initial studies on pure phases of CO_2 and CH_4 used a fixed framework model, giving a poor agreement with QENS data, leading to the development of a flexible force field for the UiO-66(Zr) framework.[74] The subsequent simulations using this force field gave a better agreement with the experiments and also allowed the elucidation of the intercage hopping mechanism of diffusion, which required a treatment of the rotation of the

dx.doi.org/10.1021/jp509672c | J. Phys. Chem. C XXXX, XXX, XXX−XXX

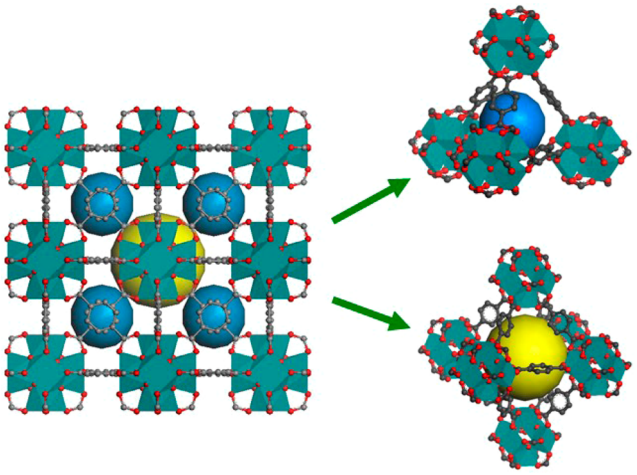

Figure 1. Illustration of the UiO-66(Zr) structure. The blue sphere and yellow sphere represent the void regions inside the tetrahedral and octahedral cages, respectively. Hydrogen atoms on the organic linkers were omitted for clarity.

phenyl rings that constitute the tetrahedral cages.[74,94] This treatment of a flexible framework also proved necessary in a study where CO_2/CH_4 mixtures in UiO-66(Zr) were considered.[73,74] In addition, functionalization of the phenyl rings can change the affinity of the framework for guest molecules as well as the diffusive properties of the adsorbates, owing to the modification of the framework's degree of flexibility. This has been illustrated during studies of CO_2 adsorption on UiO-66(Zr)-$(COOH)_2$ and of mixtures of CO_2/CH_4 and CO_2/N_2 in the same material.[50,95] Although UiO-66(Zr) and certain functionalized versions have been well-studied for the adsorption and diffusion of small gas molecules, as detailed above, the diffusion behavior of linear alkane species longer than methane through a pore system of this type, of which UiO-66(Zr) is a model material, remains unexplored.

Thus, we present a study of the adsorption and diffusion of short-chain linear hydrocarbon molecules, in the series from ethane (C2) to *n*-butane (C4). The adsorption of these gas species was first explored at room temperature by coupling manometry experiments and Grand Canonical Monte Carlo (GCMC) simulations followed by a detailed characterization of the strength of host/guest interactions involving the use of microcalorimetry measurements. The concentration dependence of the self-diffusivity of short-chain hydrocarbon molecules in UiO-66(Zr) was then explored by combining QENS measurements and MD simulations based on the use of a flexible force field for the framework. A careful analysis of the MD trajectories allows a deeper insight into the microscopic mechanism in play.

MATERIALS AND METHODS

Synthesis of UiO-66(Zr). Deuterated UiO-66(Zr) was prepared from a large-scale mixture of zirconium tetrachloride $ZrCl_4$, deuterated terephthalic acid $HO_2CC_6H_4-CO_2H$, hydrochloric acid, and dimethylformamide in the 25 mmol:50 mmol:50 mmol:150 mL ratio. The slurry was then introduced in a 750 mL Teflon liner further introduced in a metallic PAAR bomb. The system was then heated overnight (16 h) at 493 K. The resulting white product was filtered off, washed with DMF to remove the excess of unreacted terephthalic acid, then washed with acetone and dried at room temperature. The sample was finally calcined at 523 K under vacuum (5 mbar) to remove the DMF from the framework.

Adsorption Measurements. The adsorption of hydrocarbons was carried out at 303 K using a manometric adsorption apparatus coupled with a Tian-Calvet-type microcalorimeter.[96,97] This experimental device measures the isotherm and the enthalpies of adsorption simultaneously using a point by point method of gas introduction to the sample. Prior to each adsorption experiment, the UiO-66 samples were outgassed at 473 K under a vacuum of 10^{-3} mbar. The hydrocarbon gases were obtained from Air Liquide (Alphagaz, France). Each experiment was repeated several times, and both isotherms and enthalpy values were obtained by averaging over all the experiments. An error of around 0.2 kJ/mol can be assumed for the enthalpies of adsorption measured in the low loading regime.

Quasi-Elastic Neutron Scattering. The QENS experiments were carried out using the IN6 spectrometer at the ILL in Grenoble, France. An incident neutron energy of 3.12 meV (5.12 Å) was taken. The spectra were recorded at different scattering angles, the corresponding wave-vector transfers, Q, ranging from 0.25 to 1.9 $Å^{-1}$. However, the presence of strong Bragg peaks at small angles after dehydroxylation of UiO-66(Zr) restricted the number of groupings of detectors to the Q range 0.58−0.84 $Å^{-1}$. The energy transfer, $\hbar\omega$, was analyzed for ±1.5 meV. The elastic energy resolution, measured with a vanadium standard, could be fitted by a Gaussian function with a half-width at half-maximum (HWHM) varying from 41 μeV at small Q to 44 μeV at large Q.

A deuterated version of UiO-66(Zr) was used to reduce the scattering from the framework. The MOF was degassed at 473 K, and the activated solid was transferred in a glovebox into a slab-shaped aluminum container, which was connected to a gas-inlet system allowing in situ adsorption. After recording the scattering of activated UiO-66(Zr), different concentrations of C_2H_6 were investigated at 270 K, the adsorbed amounts being determined by volumetry. Measurements were performed at three temperatures for the first loading, to derive the activation energy for diffusion. Hydrogenated ethane was selected to follow the diffusion of this molecule, taking advantage of the large incoherent cross section of hydrogen.[29] The self-diffusivities were determined within an error bar of 30%.

Grand Canonical Monte Carlo and Molecular Dynamics Simulations. As a preliminary step to validate the microscopic models of both the alkanes and the MOF framework and the force field parameters for the host/guest interactions, configurational bias grand canonical Monte Carlo (CB-GCMC) simulations were conducted to predict the adsorption isotherms of C2 to C4 at 303 K using the CADSS software[98] which were further compared to the experimental data. These simulations considered a simulation box comprised of 18 (3 × 3 × 2) unit cells for UiO-66(Zr), with all atoms of the framework maintained fixed at their initial positions since the flexibility of the framework is unlikely to impact the placement of the guest molecules in the different adsorption sites by the Monte Carlo algorithm. These calculations considered 2 × 10^7 Monte Carlo (MC) steps including translation, rotation, insertion/deletion, and partial/complete regrowth of the molecule using the same acceptance probabilities as in our previous study on this series of hydrocarbons in MIL-47(V) and MIL-53(Cr).[99] The Lennard-Jones (LJ) interactions were calculated with a cutoff radius of 14.0 Å. The adsorption enthalpies at zero coverage of C1 to

dx.doi.org/10.1021/jp509672c | J. Phys. Chem. C XXXX, XXX, XXX−XXX

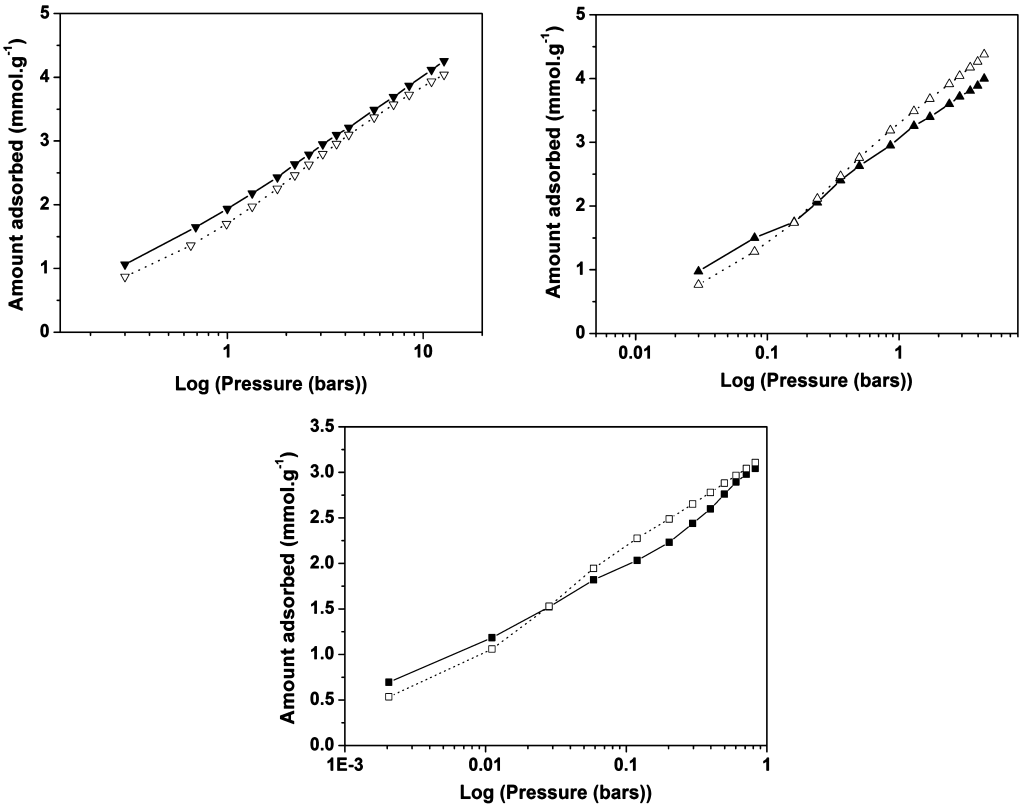

Figure 2. Experimental (empty symbols) and simulated (filled symbols) adsorption isotherms at 303 K for ethane (upside down triangles), propane (triangles), and *n*-butane (squares) in UiO-66(Zr).

C4 were calculated using the revised Widom's test particle method.[100]

Subsequently, classical MD simulations were performed to study the self-diffusivity of the short-linear alkanes in UiO-66(Zr) at 270 K using the DL_POLY 2.20 simulation package.[101] Prior to the MD simulations, 2×10^7 MC cycles in the canonical (NVT) ensemble were performed in order to randomly insert the diffusing guest molecules at the different concentrations experimentally explored. Velocities from the Maxwell−Boltzmann distribution at the required temperatures were assigned to all the adsorbate molecules and the framework atoms. The MD simulations were then conducted using the NVT ensemble at 11 different loadings for ethane, mirroring the loadings examined by QENS measurements. Seven different loadings were considered for the propane and *n*-butane calculations. On the basis of our previous findings on UiO-66(Zr) and its derivatives,[50,74,94] these MD calculations considered a fully flexible force field for the MOF framework as mentioned below, having proved important in order to capture intercage motion in a framework topology such as that of UiO-66(Zr). In the case of ethane, the MD calculations were also conducted using a rigid framework to emphasize the impact of the framework flexibility on the diffusivity. The Berendsen thermostat was used to maintain a constant temperature during the simulations.[102] Here again, the long-range Coulombic interactions were evaluated by the Ewald summation method, while all of the LJ interactions were calculated with a cutoff radius of 14.0 Å. The velocity-Verlet algorithm was used throughout to integrate Newton's equations of motion with a time step of 1 fs, and periodic boundary conditions were applied in all three dimensions. Prior to starting the production run of 2×10^7 MD steps (i.e., 20 ns), each MD system was equilibrated with at least 5×10^5 MD steps. The positions of each adsorbate molecule were stored every 5000 MD steps for subsequent analysis.

On the basis of the above simulations, we further extracted the self-diffusivity (D_s) of the guest molecules for each loading. In order to improve the statistics of the calculation, the diffusivities at each loading were averaged from five MD independent trajectories, and the method with multiple time origins was also adopted as described previously.[68] The self-diffusivity (D_s) measures the displacement of a tagged molecule as it diffuses at equilibrium, which is related to the mean squared displacement (MSD) of tagged particles by an Einstein relation[103]

$$D_s(c) = \frac{1}{2dN} \lim_{t\to\infty} \frac{d}{dt} \left\langle \sum_{i=1}^{N} |r_i(t) - r_i(0)|^2 \right\rangle \quad (1)$$

where $\langle ... \rangle$ denotes an ensemble average; $r_i(t)$ is the position vector of the diffusing molecule i at time t; N is the number of the adsorbate molecules in the simulation system; and d corresponds to the dimension of the system examined ($d = 3$ for current material).

Force Field and Charges. In this work, the alkane molecules were represented using a united atom model, where each carbon atom was grouped with its H atoms to form a single LJ site. A fixed bond length of 1.54 Å was maintained between the united atoms, and their LJ parameters were taken from the TraPPE force field.[104] The atomic partial charges used for the framework and all of the interatomic potential parameters used in the simulations are reported in Table S1 (Supporting Information). The interactions between the guest molecules and the framework, and between the guests

dx.doi.org/10.1021/jp509672c | J. Phys. Chem. C XXXX, XXX, XXX−XXX

themselves, were modeled using only LJ potentials (first term in eq 1), without any Coulombic contributions.

$$U_{ij}^{\text{nonbonded}} = 4\varepsilon_{ij}\left[\left(\frac{\sigma_{ij}}{r_{ij}}\right)^{12} - \left(\frac{\sigma_{ij}}{r_{ij}}\right)^{6}\right] + \frac{q_i q_j}{r_{ij}} \quad (2)$$

In our previous work, we verified that the simulations using the DREIDING force field[105] for the framework organic linker atoms when calculating the adsorption of CH_4 in UiO-66(Zr) lead to a better agreement with experimental data. Indeed, this force field was employed to describe the organic linkers of UiO-66(Zr), including the O atoms, while the Zr atoms were treated using the LJ parameters of the UFF force field.[106] The corresponding potential parameters for the framework atoms are listed in Table S1 (Supporting Information). All of the LJ cross-interaction parameters including adsorbent/adsorbent and adsorbate/adsorbent were determined by the Lorentz–Berthelot mixing rules.[107,108]

For the rigid framework simulations, we did not consider the LJ and Coulombic interactions between atoms of the framework because of their rigid connection with each other. In addition, only Lennard-Jones interactions between the adsorbates and between the adsorbates and the adsorbent were calculated since the united atom model for the alkanes consists of uncharged LJ sites. For the flexible framework simulations, the intraframework nonbonded interactions were modeled using the previously validated flexible force field[74,94] involving a combination of LJ and electrostatic interactions (eq 1), which were calculated only between atoms separated by more than three bonds. The Mulliken partial charges carried by all the atoms of the UiO-66(Zr) were taken from our previous density functional theory (DFT) calculation.[94] The resulting charges and the location of each atom type on the framework are described in Table S1 and Figure S1 (see Supporting Information).

RESULTS AND DISCUSSION

Adsorption. As per other adsorbates in this material,[77,79,80] including methane, the adsorption isotherms obtained experimentally are of type I, as shown in Figure 2, with a maximum loading of 4.0, 4.4, and 3.2 mmol·g^{-1} for ethane, propane, and *n*-butane, respectively, at 303 K. From these figures, one can see that the isotherms simulated using GCMC are in good agreement with those obtained by experiment in terms of the shape and the amount adsorbed, allowing a validation of the microscopic model for both host and guest, and the force field parameters used to describe the system throughout this work. It is noteworthy that this agreement is obtained using a rigid framework model for UiO-66(Zr). This clearly emphasizes that

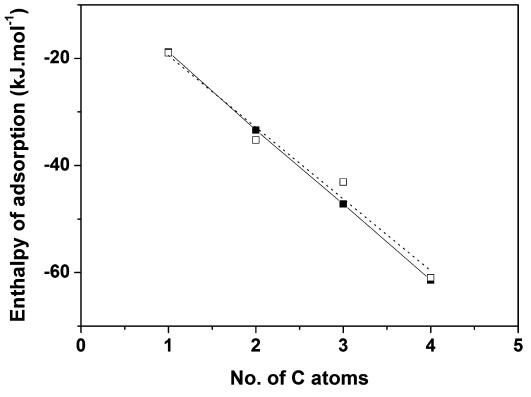

Figure 3. Plot of the adsorption enthalpy at zero coverage at 303 K against the number of carbon atoms present in the adsorbate. The experimental values are represented by the empty squares and dotted line and the simulated values by the filled squares and solid line.

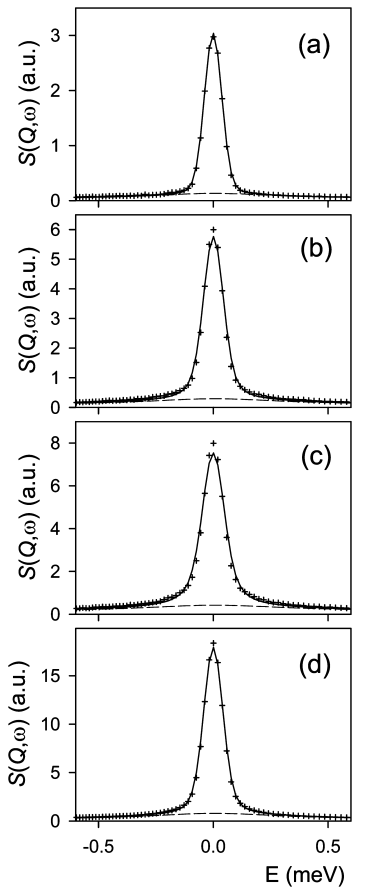

Figure 4. Comparison between the experimental (+) and the calculated spectra (solid lines) obtained for C_2H_6 in UiO-66(Zr) at various loadings: (a) 5.0, (b) 12.9, (c) 19.2, and (d) 30.7 molecules per u.c. (T = 270 K, Q = 0.61 Å^{-1}). The dashed lines indicate the contribution from rotation.

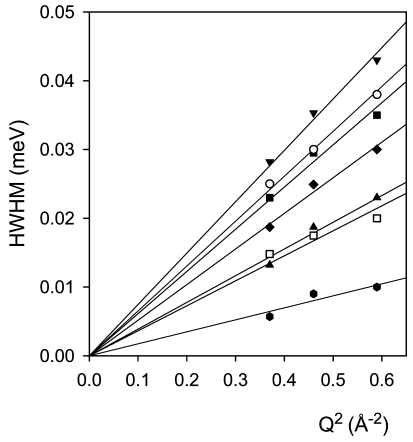

Figure 5. Half-width at half-maximum versus Q^2 of the translational component in the QENS spectra of ethane at 270 K in UiO-66(Zr) at different concentrations: 5.0 (⬢), 9.4 (▲), 12.9 (◆), 15.8 (■), 19.2 (▼), 25.8 (○), and 30.7 C_2H_6/u.c. (□).

dx.doi.org/10.1021/jp509672c | J. Phys. Chem. C XXXX, XXX, XXX–XXX

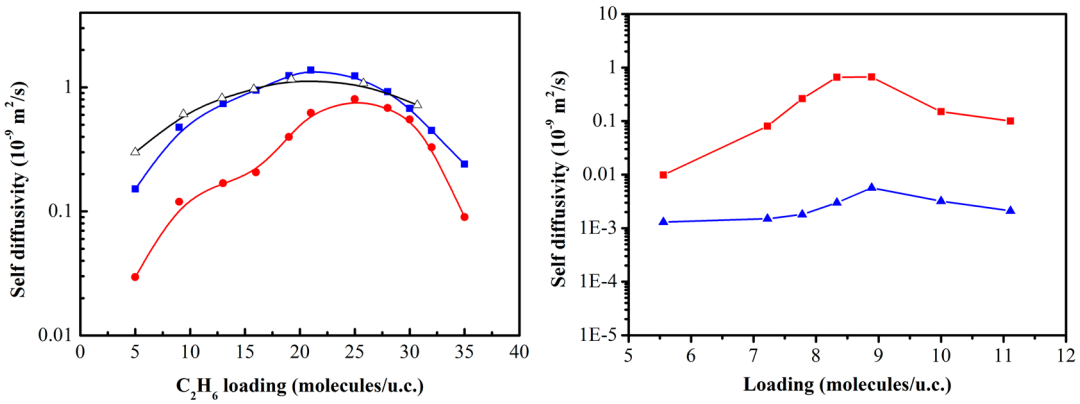

Figure 6. Left: Evolution of self-diffusion coefficients as a function of the C_2H_6 loading in UiO-66(Zr) at 270 K: QENS (empty triangles), simulations with rigid (filled circles) and flexible (filled squares) framework. Right: D_s values (from MD simulations) for propane (red squares) and *n*-butane (blue triangles) as a function of loading at 270 K.

such an assumption is reasonable when one aims to explore adsorption of molecules, even in a small pore-type MOF. This is corroborated by the good agreement between the measured adsorption enthalpy values and those calculated by GCMC at zero coverage (Figure 3). A plot of the enthalpy against the number of carbon atoms present in the adsorbate gives a linear trend (Figure 3), as already shown for the same types of hydrocarbon in other MOFs, such as MIL-53(Cr)[109] and MIL-47(V).[110] The resulting experimental (13.40 kJ/mol) and simulated (14.16 kJ/mol) incremental values are both significantly larger than the ones previously reported in the 1D-type pore channel MIL-47(V)/ML-53(Cr), which ranges from −7.5 to −10 kJ/mol. This is consistent with a stronger interaction between the additional $-CH_2$ site added as one increases the alkane length and the pore wall, due to the more confined environment of UiO-66(Zr) generated by the small pore type cages (such as the tetrahedral cages of this MOF). Inspections of the configurations extracted from the GCMC simulations for C2 to C4 at different pressures show that the adsorbates progressively fill the tetrahedral cages, which represent the most favorable adsorption sites. Once these sites are all occupied, the molecules are then adsorbed in the larger octahedral cages. Such a microscopic adsorption mechanism is consistent with the conclusions drawn from our previous studies for C1.[74,94]

Diffusion. The QENS spectra obtained at different C_2H_6 concentrations are shown in Figure 4. During a QENS experiment, one measures in $Q-\omega$ space motions which occur in real space and in time.[29] The measured intensities are proportional to a dynamical structure factor, $S(Q, \omega)$, which is the four-dimensional Fourier transform of a correlation function, $G(r,t)$, related to the translational and rotational motions of the molecule. The QENS spectra could thus be simulated by a translational scattering function convoluted with a rotational scattering function and with the instrumental resolution. The rotation was found to be isotropic, and the small radius of gyration (R = 1.52 Å) ensured a small contribution of this motion in the considered Q range (see Figure 4).

It can be seen in Figure 4 that the broadening of the elastic peak, and hence the diffusivity, increases up to a concentration of 19.2 molecules/u.c. and decreases for higher loadings. This is more evident in the plot of the HWHM as a function of Q^2 (Figure 5) where the linear variation justifies the use of a Fickian model for the diffusion. In principle, intra- and intercage motions can be differentiated by QENS (e.g., ref 21), but in the case of UiO-66(Zr), the restricted Q range did not allow a test of a more complex diffusion model. However, the convolution of this model with isotropic rotation and with the instrumental resolution already led to a good agreement with the experimental QENS spectra (see Figure 4).

Figure 6 reports the loading dependence of the self-diffusivity for ethane extracted from the above QENS spectra at 270 K. As expected from the evolution of the broadening of the elastic peak as a function of the loading (Figure 4), similarly to the case of methane,[74] the D_s presents a maximum for a loading of 19.2 molecules/u.c. and then decreases at higher concentrations. The D_s values range from 3.0×10^{-10} to 1.16×10^{-9} m^2/s, and they are significantly lower than the QENS data previously reported for methane at 230 K (from 2.0×10^{-9} to 2.80×10^{-9} m^2/s). One can also notice that the similar dependence of D_s was also experimentally found for ethane in faujasite NaX[111] with windows of larger pore sizes. Table 1 lists the D_s values for the self-diffusivity of ethane in other porous materials, obtained by means of simulation or experiments, including diverse zeolites and MOFs.

The concentration dependence of the self-diffusion coefficients of ethane in UiO-66(Zr) was further determined by MD simulations conducted using either a rigid or flexible MOF framework. Figure 6 shows that both calculations lead to a nonmonotonic profile for D_s. However, the magnitude of the QENS value in the whole range of loading and the position of the maximum are much better reproduced by the simulations considering a flexible framework. This holds also true when one compares the calculated activation energies obtained using a rigid and a flexible framework in complementary MD simulations at 200, 250, 300, and 330 K for the lowest investigated loading (5 ethane/u.c.) and using an Arrhenius plot as depicted in Figure 7. The resulting value is lower in the case of the flexible framework (7.8 vs 9.0 kJ/mol), which tends toward the QENS data for the same ethane concentration (5.0 kJ/mol). This whole observation emphasizes that in contrast to the adsorption study the dynamics of the framework in the case of small pore type MOF plays a crucial role in the diffusion of the confined molecules within their pores, and this cannot be omitted in the MD simulations. This also indicates that the force field parameters for the host/guest interactions validated on the thermodynamic properties of the system of interest lead to a very good description of the dynamic features.

dx.doi.org/10.1021/jp509672c | J. Phys. Chem. C XXXX, XXX, XXX−XXX

Table 1. Comparison of the Self-Diffusivities of Ethane, Propane, and *n*-Butane in Various Nanoporous Materials[a]

material	pore system type	adsorbate	T [K]	D_s (C_2H_6) [m^2/s]	data type	ref
FAU	3D	ethane	300	0.37−23.4	MD	16
CHA	3D	ethane	300	0.47−1.34	dcTST	114
ITQ-29 (LTA)	3D	ethane	300	0.48	MD	115
NaX	3D	ethane	300	0.87−10.10	PFG NMR	111
HKUST-1	3D	ethane	300	0.61−7.54	MD	54
MIL-53(Cr)	1D	ethane	300	3.5−15	QENS	67
MIL-53(Cr)	1D	propane	300	2.5−22	QENS	67
MIL-53(Cr)	1D	*n*-butane	300	1.5−35	QENS	67
MIL-47(V)	1D	ethane	300	6−11.5	QENS	71
MIL-47(V)	1D	propane	300	1−7.5	QENS	71
MIL-47(V)	1D	*n*-butane	300	0.8−10	QENS	71
NaY	3D	propane	300−350	1.32−2.0	MD	18
HKUST-1	3D	propane	300	3.33	MD	56
HKUST-1	3D	*n*-butane	300	2.1	MD	56
IRMOF-1	3D	propane	298	∼3	MD	113
IRMOF-1	3D	*n*-butane	298	∼3	MD	113
UiO-66(Zr)	cage	ethane	270	0.30−1.16	QENS	this work
			270	0.15−1.38	MD (Flexible)	this work
			270	0.03−0.80	MD (Rigid)	this work
		propane	270	0.01−0.17	MD (Flexible)	this work
		n-butane	270	0.00167−0.0077	MD (Flexible)	this work
silicalite	2D	ethane	300	0.33−6.21	MD	31
				0.50−5.00	PFG NMR	42
zeolite X	3D	ethane	300	1.00−10.00	PFG NMR	42
zeolite A	3D	ethane	300	0.10−0.40	PFG NMR	42
MFI	2D	ethane	300	0.71−7.34	MD	16
Si-MFI	2D	ethane	300	0.68−7.37	MD	111
				0.47−5.12	PFG NMR	111
ISV	3D	ethane	300	0.09−18.47	MD	16
BEA	3D	ethane	300	3.48−29.21	MD	16
FER	2D	ethane	300	0.17−14.31	MD	16
Si-AFI	1D	ethane	300	1.09−23.00	MD	111
Si-CHA	3D	ethane	301	0.000480	PFG NMR	43
Si-LTA	3D	ethane	300	0.02−1.05	MD	111
LTA-5A	3D	ethane	300	0.10−0.38	PFG NMR	111
Si-IHW	2D	ethane	300	0.04	MD	115
Si-ITE	2D	ethane	300	0.43	MD	115
sol−gel derived silica		ethane	200	0.43 ± 0.05	QENS	40
			235	2.9 ± 0.22	QENS	40
			270	5.3 ± 0.35	QENS	40
NaZSM-5	2D	ethane	300	1.25−3.00	QENS	35
NaX	3D	ethane	223	0.25−2.40	PFG NMR	39
NaA	3D	ethane	350	0.0000113−0.0000170	MCLD	25
SAPO-34	1D	ethane	295	0.0044−0.0067	PFG NMR	41
Zn(tbip)	1D	ethane	298	0.9−1.5	MD	62
			300	0.07−1.03	MD	61
MOF-5	3D	ethane	298	21.0	PFG NMR	57
			223	19.0	PFG NMR	57
Cu-BTC	3D	ethane	300	6.7	MD	56
Co-FA		ethane	300	0.0020−0.11	MD	17
Mn-FA		ethane	300	0.015−0.46	MD	17
ZIF-8	3D	ethane	298	0.00876−0.00915	IRM	55
ALPO-5		ethane	300	1.6−1.8	MD	9
silicalite-1B	2D	butane	298	8−9	PFG NMR	27
LTL	3D	ethane	300	5	MD/dcTST	26
LTL	3D	propane	300	3	MD/dcTST	26

[a]Here, the QENS and PFG NMR data are related to intracrystalline and to both intra- and intercrystalline diffusion processes, respectively. However, this difference can be counteracted by using sufficiently large crystallites, which is generally the case if the studies are focused on intracrystalline diffusion.[112]

dx.doi.org/10.1021/jp509672c | J. Phys. Chem. C XXXX, XXX, XXX−XXX

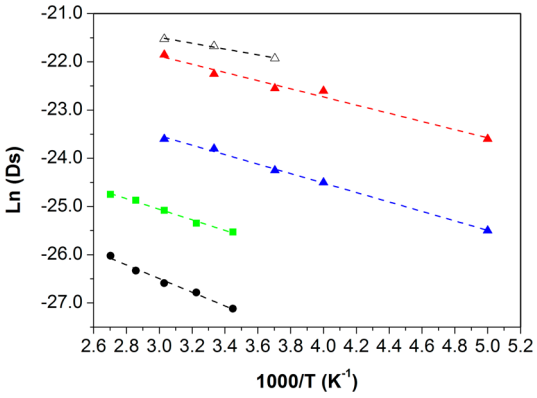

Figure 7. Simulated self-diffusivities (expressed in $m^2\ s^{-1} \times 10^{-8}$) for ethane with rigid (blue filled triangles) and flexible (red filled triangles) framework at 200, 250, 270, 300, and 330 K used for calculating the activation energies. The data for propane (green filled squares) and *n*-butane (black filled circles) are also shown at 290, 310, 330, 350, and 370 K for a loading of five molecules per unit cell. The QENS data are reported as black empty triangles.

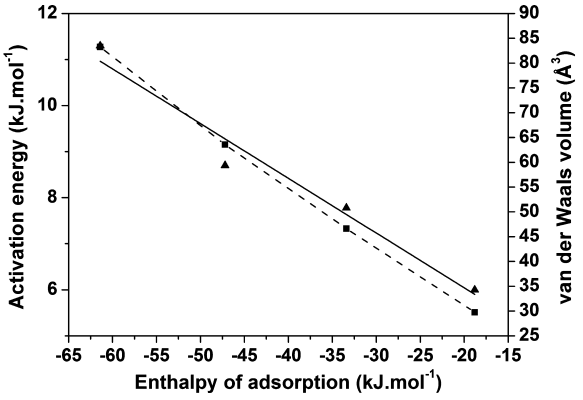

Figure 8. Plot of the simulated activation energies (squares and dotted line) and the van der Waals volume (triangles and solid line) against the calculated adsorption enthalpies at low coverage for all alkanes.

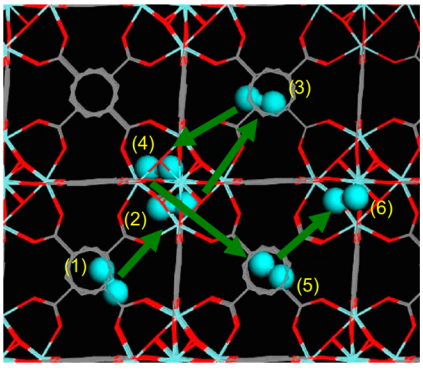

Figure 9. Illustration of the diffusion mechanism of C_2H_6 in UiO-66(Zr) at a loading of 5 molecules/u.c.. The positions 1−6 denote the jump sequences of C_2H_6 observed during the MD trajectory.

The self-diffusivities further simulated for the propane and *n*-butane cases show the same trends as ethane, as a function of concentration with a maximum shifted to a lower loading, i.e., 9 molecules/u.c. (see Figure 6). The resulting D_s are at least one order of magnitude smaller than those obtained for ethane, with values ranging from 1×10^{-11} to 1.7×10^{-10} $m^2\ s^{-1}$ and from 1.67×10^{-12} to 7.7×10^{-12} $m^2\ s^{-1}$ for propane and *n*-butane, respectively. This is consistent with the general finding that smaller molecules will diffuse faster in a given host material than larger ones, regardless of the pore topology. A comparison of these D_s values with those obtained in different MOFs included (see Table 1) shows that these adsorbates diffuse slowly in UiO-66(Zr) by at least one order of magnitude, showing the effect of the UiO-66(Zr) pore topology on the diffusion, as compared to channel-containing MOFs. The activation energies for propane and *n*-butane were also calculated in the same manner, using a flexible framework model only, with a loading of 5 molecules/u.c. (see Figure 7 for the corresponding Arrhenius plots). For propane, a value of 8.7 kJ/mol was obtained, while 11.3 kJ/mol was calculated for the *n*-butane case. Both values are higher than the ones previously obtained for the same alkanes in the open channel MOFs including MIL-47(V), MIL-53(Cr), HKUST-1, and IRMOF-1 which range from 3 to 8.5 kJ/mol,[55,65,108,113] consistent with the higher degree of confinement in the tetrahedral cages of UiO-66(Zr).

In keeping with the methane and ethane analysis, the activation energy therefore increases linearly as a function of the adsorption enthalpy at low coverage, as shown in Figure 8. This illustrates that increasing the hydrocarbon length leads to a stronger retention in the tetrahedral cages which correspond to the preferential siting sites for all alkanes, leading to a higher activation energy for diffusion. This trend is consistent with the increase of the van der Waals volume estimated for each alkane (see Figure 8) and thus confirms that in this host system the degree of confinement strongly affects the molecule's capacity to diffuse.

To obtain more insight into the diffusion mechanism of these longer chain alkanes, the diffusion trajectories of ethane were first carefully studied. It was observed that at low loading the mobility of these molecules occurs via intracage motions inside tetrahedral cages or by jump sequences "tetrahedral cages−octahedral cages−tetrahedral cages" through triangular windows, as schematically illustrated in Figure 9. Ethane obeys a 3D-type diffusion mechanism from a translational point of view, and an analysis of the trajectories extracted from the simulations shows that during the periods where the ethane molecules reside in the tetrahedral cages the diffusive species are orientated in a random fashion, which is consistent with the isotropic rotational dynamics evidenced from the fit of the QENS spectra. It was further shown that the ethane molecules spend most of their time in the tetrahedral cages and quickly jump back or into another tetrahedral cage once they enter the octahedral cage.

The 2D probability density distributions for ethane were calculated at different loadings from the MD trajectories recorded at 270 K. As shown in Figure 10a, these species mostly distribute in the tetrahedral cages at the loading of 5 molecules/u.c. Because the size of tetrahedral cages is smaller than those of the octahedral cages, the alkanes more easily interact with the walls of the tetrahedral cages so are more likely to be adsorbed in these cages at low loading, as described above. At intermediate loadings (Figure 10b), the tetrahedral cages are still preferentially occupied, and some molecules start to diffuse over longer distances into the adjacent octahedral cages, thus leading to an increase of D_s, which passes through a maximum. This proposition coincides with the D_s vs loading profile shown in Figure 6. At high loadings (Figure 10c), both tetrahedral cages and octahedral cages are nearly fully occupied by C_2H_6 molecules, and the D_s values are low. A similar

dx.doi.org/10.1021/jp509672c | J. Phys. Chem. C XXXX, XXX, XXX−XXX

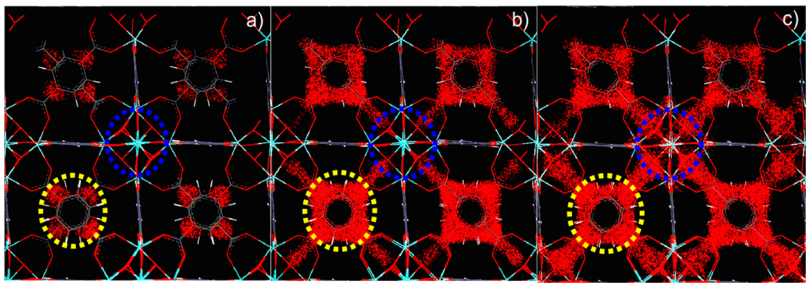

Figure 10. 2D probability density plots of the COM of C_2H_6 in UiO-66(Zr) at 270 K from MD at different loadings. (a) 5 molecules/u.c., (b) 21 molecules/u.c., (c) 35 molecules/u.c. (Yellow and blue circles denote the tetrahedral and octahedral cages, respectively.)

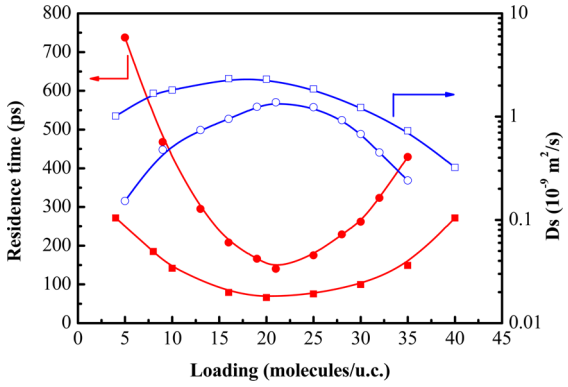

Figure 11. D_s (empty symbols) and residence time (filled symbols) for C_2H_6 (circle symbols) in tetrahedral cages of flexible UiO-66(Zr) at 230 and 270 K, respectively. For comparison, the same data previously obtained for CH_4 (square symbols) are represented.[74]

behavior is seen for propane and *n*-butane in Figures S2 and S3 (Supporting Information). Propane and *n*-butane molecules also diffuse via the same jump sequence mechanism. As for the ethane molecules, these molecules must pass through the triangular windows when migrating from a tetrahedral cage to an octahedral cage, which becomes increasingly difficult as one increases the van der Waals volume of the molecules, as illustrated by the activation energies and decreasing D_s values discussed above. Since the larger molecules have a higher activation energy, this slows the molecule in its diffusion path through the pore system of the MOF.

To further provide an interpretation of the concentration dependence of D_s, the average residence time inside the tetrahedral cages of the UiO-66(Zr) material was calculated for all alkanes as a function of loading, using the trajectories recorded during the MD runs. In each calculation, the starting coordinates of all the molecules stored in one MD trajectory were employed to determine whether the guests are located inside or outside the tetrahedral cages using the center positions and diameters of all of these types of cages. The subsequent coordinates of all the molecules were used to follow whether they enter or leave these cages. If some molecules that were initially inside a tetrahedron were found to move out of these cages, the time intervals between their entrance and the current moment were then calculated. As shown in Figure 11, the profiles of residence time and D_s are both nonmonotonic curves, and a minimum of residence time is obtained when the D_s curve reaches the maximum in a similar way to what was previously observed for methane. Therefore, the D_s of guest molecules in porous materials may be linked to the residence time values. As may be inferred from Figure 10, in the low loading range, the ethane molecules are mostly distributed in tetrahedral cages, interacting with the framework, leading to low D_s values and long residence times. With an increase in loading, the adsorbates become freer to diffuse into the adjacent octahedral cages, hence the increase in D_s values and, accordingly, the decrease in residence times. When the loading increases to a certain extent, both the tetrahedral cages and the octahedral cages become increasingly occupied, hindering the diffusion of the guests. Therefore, the D_s values decrease, and the residence time increases with the increase in loading. The same explanation also holds for the propane and *n*-butane cases. However, with *n*-butane, although we obtain the same shape for the D_s vs loading curve, one can see that this curve is much flatter, explaining the smaller variation of D_s with loading. This indicates that *n*-butane molecules initially located in the tetrahedral cages diffuse less readily than the shorter alkanes.

CONCLUSIONS

This work describes the diffusion of ethane, propane, and *n*-butane in UiO-66(Zr) by means of QENS measurements and MD simulations based on a force field preliminarily validated with the adsorption data collected by gravimetry/calorimetry measurements. The simulated self-diffusivities of ethane are in good agreement with those measured by QENS, and both sets of data present a nonmonotonic profile with the presence of a maximum. The same concentration dependence profile for D_s was further predicted for propane and *n*-butane, although the maximum decreases to a lower concentration, given the larger size of these molecules. The profile of residence time for all alkanes in the tetrahedral cages of UiO-66(Zr) was further simulated for the interpretation of the self-diffusivity profile. It was shown that the diffusion of these guest molecules is an isotropic process with 3D-type jumping behavior from tetrahedral to octahedral cages. The more bulky molecules were revealed to diffuse more slowly through the pores. The order of the diffusion coefficients decreases with increasing van der Waals volume, increasing adsorption enthalpy at low coverage, and increasing activation energy, which illustrates that the diffusivity in this cage-type MOF is predominantly governed by the degree of confinement of the molecule in the pore.

ASSOCIATED CONTENT

Supporting Information

Self-diffusivities of C_2H_6 in other nanoporous materials. This material is available free of charge via the Internet at http://pubs.acs.org.

dx.doi.org/10.1021/jp509672c | J. Phys. Chem. C XXXX, XXX, XXX−XXX

AUTHOR INFORMATION

Corresponding Authors

*E-mail: naseem.ramsahye@enscm.fr.

*E-mail: qyyang@mail.buct.edu.cn.

Notes

The authors declare no competing financial interest.

ACKNOWLEDGMENTS

The authors are very grateful to Dr. Thomas Devic for very useful discussions and thank the Institut Laue−Langevin for allocating neutron beam time on IN6. G.M. thanks the Institut Universitaire de France for its support. This work was also supported by the National Key Basic Research Program of China ("973") (No. 2013CB733503), the Natural Science Foundation of China (Nos. 21136001 and 21322603), and the Program for New Century Excellent Talents in University (No. NCET-12-0755), as well as the European Community's Seventh Framework Programme (FP7/2007-2013 "MACADEMIA") under Grant Agreement 228862.

REFERENCES

(1) Li, J.; Sculley, J.; Zhou, H.-C. Metal-Organic Frameworks for Separations. *Chem. Rev.* **2012**, *112*, 869−932.

(2) Bloch, E. D.; Queen, W. L.; Krishna, R.; Zadrozny, J. M.; Brown, C. M.; Long, J. R. Hydrocarbon Separations in a Metal-Organic Framework with Open iron(II) Coordination Sites. *Science* **2012**, *335*, 1606−1610.

(3) Wu, H.; Gong, Q.; Olson, D. H.; Li, J. Commensurate Adsorption of Hydrocarbons and Alcohols in Microporous Metal Organic Frameworks. *Chem. Rev.* **2012**, *112*, 836−868.

(4) Mueller, U.; Schubert, M.; Teich, F.; Puetter, H.; Pastre, J. Metal−organic Frameworks — Prospective Industrial Applications. *J. Mater. Chem.* **2006**, *16*, 626−636.

(5) Herm, Z. R.; Bloch, E. D.; Long, R. Hydrocarbon Separations in Metal−Organic Frameworks. *Chem. Mater.* **2014**, *26*, 323−338.

(6) Denayer, J. F. M.; Devriese, L. I.; Couck, S.; Martens, J.; Singh, R.; Webley, P. A.; Baron, G. V. Cage and Window Effects in the Adsorption of N-Alkanes on Chabazite and SAPO-34. *J. Phys. Chem. C* **2008**, *112*, 16593−16599.

(7) Jiang, J.; Sandler, S. I.; Schenk, M.; Smit, B. Adsorption and Separation of Linear and Branched Alkanes on Carbon Nanotube Bundles from Configurational-Bias Monte Carlo Simulation. *Phys. Rev. B* **2005**, *72*, 045447−1−045447−11.

(8) Demontis, P.; Fenu, L. A. A.; Suffritti, G. B. B. Diffusion in Confined Systems: Methane in a ZK4Molecular Sieve. A Molecular Dynamics Simulation Study. *J. Phys. Chem. B* **2005**, *108*, 18081−18087.

(9) Demontis, P.; Gonzalez, J. G.; Suffritti, G. B. Statics and Dynamics of Ethane Molecules in AlPO4−5: A Molecular Dynamics Simulations Study. *J. Am. Chem. Soc.* **2001**, *123*, 5069−5074.

(10) Demontis, P.; Suffritti, G. B. Structure and Dynamics of Zeolites Investigated by Molecular Dynamics. *Chem. Rev.* **1997**, *97*, 2845−2878.

(11) Demontis, P.; Suffritti, G. B. . A Molecular Dynamics Study of Diffusion of Methane in Partially Dealuminated Zeolite NaA. *Mol. Phys.* **1997**, *91*, 669−679.

(12) Beerdsen, E.; Dubbeldam, D.; Smit, B. Loading Dependence of the Diffusion Coefficient of Methane in Nanoporous Materials. *J. Phys. Chem. B* **2006**, *110*, 22754−22772.

(13) Beerdsen, E.; Dubbeldam, D.; Smit, B. Understanding Diffusion in Nanoporous Materials. *Phys. Rev. Lett.* **2006**, *96*, 044501.

(14) Beerdsen, E.; Smit, B.; Dubbeldam, D. Molecular Simulation of Loading Dependent Slow Diffusion in Confined Systems. *Phys. Rev. Lett.* **2004**, *93*, 248301.

(15) Garcia-Sanchez, A.; Dubbeldam, D.; Calero, S. Modeling Adsorption and Self-Diffusion of Methane in LTA Zeolites: The Influence of Framework Flexibility. *J. Phys. Chem. C* **2010**, *114*, 15068−15074.

(16) Krishna, R.; van Baten, J. M. A Molecular Dynamic Investigation of the Diffusion of Methane-Ethane and Methane-Propane Mixtures in Zeolites. *Chem. Eng. Technol.* **2006**, *29*, 1429−1437.

(17) Krishna, R.; van Baten, J. M. A Molecular Simulation Study of Commensurate−incommensurate Adsorption of N-Alkanes in Cobalt Formate Frameworks. *Mol. Simul.* **2009**, *35*, 1098−1104.

(18) Yashonath, S.; Demontis, P.; Klein, M. L. Temperature and Concentration Dependence of Adsorption Properties of Methane in Nay: A Molecular Dynamics Study. *J. Phys. Chem.* **1991**, *95*, 5881−5889.

(19) Sayeed, A.; Mitra, S.; Anil Kumar, a. V.; Mukhopadhyay, R.; Yashonath, S.; Chaplot, S. L. Diffusion of Propane in Zeolite NaY: A Molecular Dynamics and Quasi-Elastic Neutron Scattering Study. *J. Phys. Chem. B* **2003**, *107*, 527−533.

(20) Clark, L. A.; Ye, G. T.; Gupta, A.; Hall, L. L.; Snurr, R. Q. Diffusion Mechanisms of Normal Alkanes in Faujasite Zeolites. *J. Chem. Phys.* **1999**, *111*, 1209−1222.

(21) Deroche, I.; Maurin, G.; Borah, B. J.; Yashonath, S.; Jobic, H. Diffusion of Pure CH 4 and Its Binary Mixture with CO 2 in Faujasite NaY: A Combination of Neutron Scattering Experiments and Molecular Dynamics Simulations. *J. Phys. Chem. C* **2010**, *114*, 5027−5034.

(22) Chempath, S.; Krishna, R.; Snurr, R. Q. Non-Equilibrium Molecular Dynamics Simulations of Diffusion of Binary Mixtures Containing Short N-Alkanes in Faujasite. *J. Phys. Chem. B* **2004**, *108*, 13481−13491.

(23) Rives, S.; Jobic, H.; Beale, A. M.; Maurin, G. Diffusion of CH4, CO2, and Their Mixtures in AlPO4−5 Investigated by QENS Experiments and MD Simulations. *J. Phys. Chem. C* **2013**, *117*, 13530−13539.

(24) Hussain, I.; Titiloye, J. O. Molecular Dynamics Simulations of the Adsorption and Diffusion Behavior of Pure and Mixed Alkanes in Silicalite. *Microporous Mesoporous Mater.* **2005**, *85*, 143−156.

(25) Gladden, L. F.; Sousa-Goncalves, J. A.; Alexander, P. Adsorption and Transport of Ethane and Ethene in Zeolite NaA: 2 H NMR and Monte Carlo Lattice Dynamics Studies. *J. Phys. Chem. B* **1997**, *101*, 10121−10127.

(26) Dubbeldam, D.; Beerdsen, E.; Vlugt, T. J. H.; Smit, B. Molecular Simulation of Loading-Dependent Diffusion in Nanoporous Materials Using Extended Dynamically Corrected Transition State Theory. *J. Chem. Phys.* **2005**, *122*, 224712.

(27) Jobic, H.; Schmidt, W.; Krause, C. B.; Karger, J. PFG NMR and QENS Diffusion Study of N-Alkane Homologues in MFI-Type Zeolites. *Microporous Mesoporous Mater.* **2006**, *90*, 299−306.

(28) Binder, T.; Chmelik, C.; Kärger, J.; Martinez-Joaristi, A.; Gascon, J.; Kapteijn, F.; Ruthven, D. A Diffusion Study of Small Hydrocarbons in DDR Zeolites by Micro-Imaging. *Microporous Mesoporous Mater.* **2013**, *180*, 219−228.

(29) Jobic, H.; Theodorou, D. N. Quasi-Elastic Neutron Scattering and Molecular Dynamics Simulation as Complementary Techniques for Studying Diffusion in Zeolites. *Microporous Mesoporous Mater.* **2007**, *102*, 21−50.

(30) Jobic, H.; Hahn, K.; Karger, J.; Bee, M.; Tuel, A.; Noack, M.; Gimus, I.; Kearley, G. J. Unidirectional and Single-File Diffusion of Molecules in One-Dimensional Channel Systems: A Quasi-Elastic Neutron Scattering Study. *J. Phys. Chem. B* **1997**, *101*, 5834−5841.

(31) Chong, S. S.; Jobic, H.; Plazanet, M.; Sholl, D. S. Concentration Dependence of Transport Diffusion of Ethane in Silicalite: A Comparison between Neutron Scattering Experiments and Atomically Detailed Simulations. *Chem. Phys. Lett.* **2005**, *408*, 157−161.

(32) Jobic, H. On the Jump Diffusion of Molecules in Zeolites Measured by Quasi-Elastic Neutron Scattering. *Microporous Mesoporous Mater.* **2002**, *55*, 159−169.

(33) Gergidis, L. N.; Theodorou, D. N.; Jobic, H. Dynamics of N-Butane-Methane Mixtures in Silicalite, Using Quasielastic Neutron Scattering and Molecular Dynamics Simulations. *J. Phys. Chem. B* **2000**, *104*, 5541−5552.

(34) Jobic, H.; Bee, M.; Kearley, G. J. Mobility of Methane in Zeolite NaY between 100 and 250K - A Quasi-Elastic Neutron-Scattering Study. *J. Phys. Chem.* **1994**, *98*, 4660−4665.
(35) Jobic, H.; Bee, M.; Kearley, G. J. Dynamics of Ethane and Propane in Zeolite ZSM-5 Studied by Quasi-Elastic Neutron-Scattering. *Zeolites* **1992**, *12*, 146−151.
(36) Benes, N. E.; Jobic, H.; Vverweij, H. Quasi-Elastic Neutron Scattering Study of the Mobilit of Methane in Microporous Silica. *Microporous Mesoporous Mater.* **2001**, *43*, 147.
(37) Vasenov, S.; Bohlmann, W.; Galvosas, P.; Geier, O.; Liu, H.; Karger, J. PFG NMR Study of Diffusion in MFI-Type Zeolites: Evidence of the Existence of Intracrystalline Transport Barriers. *J. Phys. Chem. B* **2001**, *105*, 5922−5927.
(38) Jost, S.; Bar, N. K.; Fritzsche, S.; Haberlandt, R.; Karger, J. Diffusion of a Mixture of Methane and Xenon in Silicalite: A Molecular Dynamics Study and Pulsed Field Gradient Nuclear Magnetic Resonance Experiments. *J. Phys. Chem. B* **1998**, *102*, 6375−6381.
(39) Karger, J.; Pfeifer, H.; Rauscher, M.; Walter, A. Self-Diffusion of N-Paraffins in NaX Zeolite. *J. Chem. Soc., Faraday Trans. I* **1980**, *76*, 717−737.
(40) Dewitt, A. C.; Herwig, K. W.; Lombardo, S. J. Adsorption and Diffusion Behavior of Ethane and Ethylene in Sol-Gel Derived Microporous Silica. *Adsorption* **2005**, *11*, 491−499.
(41) Dai, W.; Scheibe, M.; Li, L.; Guan, N.; Hunger, M. Effect of the Methanol-to-Olefin Conversion on the PFG NMR Self-Diffusivities of Ethane and Ethene in Large-Crystalline SAPO-34. *J. Phys. Chem. C* **2012**, *116*, 2469−2476.
(42) Caro, J.; Bulow, M.; Schirmer, W.; Karger, J.; Heink, W.; Pfeifer, H.; Zdanov, S. P. Microdynamics of Methane, Ethane and Propane in ZSM-5 Type Zeolites. *J. Chem. Soc., Faraday Trans. I* **1985**, *81*, 2541−2550.
(43) Hedin, N.; Demartin, G. J.; Roth, W. J.; Strohmaier, K. G. PFG NMR Self-Diffusion of Small Hydrocarbons in High Silica DDR, CHA and LTA Structures. *Microporous Mesoporous Mater.* **2008**, *109*, 327−334.
(44) Sumida, K.; Rogow, D. L.; Mason, J. a; McDonald, T. M.; Bloch, E. D.; Herm, Z. R.; Bae, T.-H.; Long, J. R. Carbon Dioxide Capture in Metal-Organic Frameworks. *Chem. Rev.* **2012**, *112*, 724−781.
(45) He, Y.; Zhou, W.; Qian, G.; Chen, B. Methane Storage in Metal-Organic Frameworks. *Chem. Soc. Rev.* **2014**, *43*, 5657−5678.
(46) Mason, J. a.; Veenstra, M.; Long, J. R. Evaluating Metal−organic Frameworks for Natural Gas Storage. *Chem. Sci.* **2014**, *5*, 32−51.
(47) Suh, M. P.; Park, H. J.; Prasad, T. K.; Lim, D.-W. Hydrogen Storage in Metal-Organic Frameworks. *Chem. Rev.* **2012**, *112*, 782−835.
(48) Rives, S.; Jobic, H.; Ragon, F.; Devic, T.; Serre, C.; Férey, G.; Ollivier, J.; Maurin, G. Diffusion of Long Chain N-Alkanes in the Metal−organic Framework MIL-47(V): A Combination of Neutron Scattering Experiments and Molecular Dynamics Simulations. *Microporous Mesoporous Mater.* **2012**, *164*, 259−265.
(49) Férey, G. Hybrid Porous Solids: Past, Present, Future. *Chem. Soc. Rev.* **2008**, *37*, 191−214.
(50) Yang, Q.; Vaesen, S.; Ragon, F.; Wiersum, A. D.; Wu, D.; Lago, A.; Devic, T.; Martineau, C.; Taulelle, F.; Llewellyn, P. L.; et al. A Water Stable Metal-Organic Framework with Optimal Features for CO2 Capture. *Angew. Chem., Int. Ed. Engl.* **2013**, *52*, 10316−10320.
(51) Czaja, A. U.; Trukhan, N.; Muller, U. Industrial Applications of Metal-Organic Frameworks. *Chem. Soc. Rev.* **2009**, *38*, 1284−1293.
(52) Voorde, B. Van De; Bueken, B.; Vos, D. De. Adsorptive Separation on Metal−organic Frameworks in the Liquid Phase. *Chem. Soc. Rev.* **2014**, *43*, 5766−5788.
(53) Lu, W.; Wei, Z.; Gu, Z.-Y.; Liu, T.-F.; Park, J.; Park, J.; Tian, J.; Zhang, M.; Zhang, Q.; Gentle Iii, T.; et al. Tuning the Structure and Function of Metal-Organic Frameworks via Linker Design. *Chem. Soc. Rev.* **2014**, *43*, 5561−5593.
(54) Chmelik, C.; Kärger, J.; Wiebcke, M.; Caro, J.; van Baten, J. M.; Krishna, R. Adsorption and Diffusion of Alkanes in CuBTC Crystals Investigated Using Infra-Red Microscopy and Molecular Simulations. *Microporous Mesoporous Mater.* **2009**, *117*, 22−32.
(55) Chmelik, C.; Bux, H.; Caro, J.; Heinke, L.; Hibbe, F.; Titze, T.; Karger, J. Mass Transfer in a Nanoscale Material Enhanced by an Opposing Flux. *Phys. Rev. Lett.* **2010**, *104*, 085902.
(56) Wehring, M.; Gascon, J.; Dubbeldam, D.; Kapteijn, F.; Snurr, R. Q.; Stallmach, F. Self-Diffusion Studies in CuBTC by PFG NMR and MD Simulations. *J. Phys. Chem. C* **2010**, *114*, 10527−10534.
(57) Stallmach, F.; Gröger, S.; Künzel, V.; Kärger, J.; Yaghi, O. M.; Hesse, M.; Müller, U. NMR Studies on the Diffusion of Hydrocarbons on the Metal-Organic Framework Material MOF-5. *Angew. Chem., Int. Ed. Engl.* **2006**, *45*, 2123−2126.
(58) Chmelik, C.; Freude, D.; Bux, H.; Haase, J. Ethene/ethane Mixture Diffusion in the MOF Sieve ZIF-8 Studied by MAS PFG NMR Diffusometry. *Microporous Mesoporous Mater.* **2012**, *147*, 135−141.
(59) Skoulidas, A. I.; Scholl, D. S. Self-Diffusion and Transport Diffusion of Light Gases in Metal-Organic Framework Materials Assessed Using Molecular Dynamics Simulations. *J. Phys. Chem. B* **2005**, *109*, 15760−15768.
(60) Seehamart, K.; Nanok, T.; Kärger, J.; Chmelik, C.; Krishna, R.; Fritzsche, S. Investigating the Reasons for the Significant Influence of Lattice Flexibility on Self-Diffusivity of Ethane in Zn(tbip). *Microporous Mesoporous Mater.* **2010**, *130*, 92−96.
(61) Seehamart, K.; Nanok, T.; Krishna, R.; Baten, J. M.; Van Remsungnen, T.; Fritzsche, S. A Molecular Dynamics Investigation of the Influence of Framework Flexibility on Self-Diffusivity of Ethane in Zn(tbip) Frameworks. *Microporous Mesoporous Mater.* **2009**, *125*, 97−100.
(62) Seehamart, K.; Chmelik, C.; Krishna, R.; Fritzsche, S. Microporous and Mesoporous Materials Molecular Dynamics Investigation of the Self-Diffusion of Binary Mixture Diffusion in the Metal-Organic Framework Zn (Tbip) Accounting for Framework Flexibility. *Microporous Mesoporous Mater.* **2011**, *143*, 125−131.
(63) Babarao, R.; Tong, Y. H.; Jiang, J. J. W. Molecular Insight into Adsorption and Diffusion of Alkane Isomer Mixtures in Metal-Organic Frameworks. *J. Phys. Chem. B* **2009**, *113*, 9129−9136.
(64) Krishna, R.; van Baten, J. M. Highlighting a Variety of Unusual Characteristics of Adsorption and Diffusion in Microporous Materials Induced by Clustering of Guest Molecules. *Langmuir* **2010**, *26*, 8450−8463.
(65) Salles, F.; Jobic, H.; Devic, T.; Guillerm, V.; Serre, C.; Koza, M. M.; Ferey, G.; Maurin, G. Diffusion of Binary CO2/CH4Mixtures in the MIL-47(V) and MIL-53(Cr) Metal-Organic Framework Type Solids: A Combination of Neutron Scattering Measurements and Molecular Dynamics Simulations. *J. Phys. Chem. C* **2013**, *117*, 11275−11284.
(66) Deroche, I.; Rives, S.; Trung Khuong, T.; Yang, Q.; Ghoufi, A.; Ramsahye, N. A.; Trens, P.; Fajula, F.; Devic, T.; Serre, C.; et al. Exploration of the Long-Chain N-Alkanes Adsorption and Diffusion in the MOF-Type MIL-47 (V) Material by Combining Experimental and Molecular Simulation Tools. *J. Phys. Chem. C* **2011**, *115*, 13868−13876.
(67) Rosenbach, N., Jnr; Jobic, H.; Ghoufi, A.; Devic, T.; Koza, M. M.; Ramsahye, N. A.; Mota, C. J.; Serre, C.; Maurin, G. Diffusion of Light Hydrocarbons in the Flexible MIL-53(Cr) Metal−Organic Framework: A Combination of Quasi-Elastic Neutron Scattering Experiments and Molecular Dynamics Simulations. *J. Phys. Chem. C* **2014**, *118*, 14471−14477.
(68) Salles, F.; Jobic, H.; Ghoufi, A.; Llewellyn, P. L.; Serre, C.; Bourrelly, S.; Férey, G.; Maurin, G. Transport Diffusivity of CO2 in the Highly Flexible Metal-Organic Framework MIL-53(Cr). *Angew. Chem., Int. Ed. Engl.* **2009**, *48*, 8335−8339.
(69) Rives, S.; Jobic, H.; Ollivier, J.; Yang, K. Diffusion of Branched and Linear C 6 -Alkanes in the. *J. Phys. Soc. Jpn.* **2013**, *82*, SA005−1−SA005−13.
(70) Rives, S.; Trung, T.; Yang, Q.; Ghou, A.; Ramsahye, N. A.; Trens, P.; Fajula, F.; Devic, T.; Serre, C.; Jobic, H.; et al. Exploration of the Long-Chain N -Alkanes Adsorption and Diffusion in the MOF-

Type MIL-47 (V) Material by Combining Experimental and Molecular Simulation Tools. *J. Phys. Chem. C* **2011**, *115*, 13868−13876.
(71) Jobic, H.; Rosenbach, N.; Ghoufi, A.; Kolokolov, D. I.; Yot, P. G.; Devic, T.; Serre, C.; Férey, G.; Maurin, G. Unusual Chain-Length Dependence of the Diffusion of N-Alkanes in the Metal-Organic Framework MIL-47(V): The Blowgun Effect. *Chem.—Eur. J.* **2010**, *16*, 10337−10341.
(72) Pantatosaki, E.; Jobic, H.; Kolokolov, D. I.; Karmakar, S.; Bibiwale, R.; Papadopoulos, G. K. Probing the Hydrogen Equilibrium and Kinetics in Zeolite Imidazolate Frameworks via Molecular Dynamics and Quasi-Elastic Neutron Scattering Experiments. *J. Chem. Phys.* **2013**, *138*, 034706.
(73) Yang, Q.; Wiersum, A. D.; Jobic, H.; Guillerm, V.; Serre, C.; Llewellyn, P. L. P. L.; Maurin, G. Understanding the Thermodynamic and Kinetic Behavior of the CO2/CH4 Gas Mixture within the Porous Zirconium Terephthalate UiO-66(Zr): A Joint Experimental and Modeling Approach. *J. Phys. Chem. C* **2011**, *115*, 13768−13774.
(74) Yang, Q.; Jobic, H.; Salles, F.; Kolokolov, D.; Guillerm, V.; Serre, C.; Maurin, G. Probing the Dynamics of CO2 and CH4 within the Porous Zirconium Terephthalate UiO-66(Zr): A Synergic Combination of Neutron Scattering Measurements and Molecular Simulations. *Chem.—Eur. J.* **2011**, *17*, 8882−8889.
(75) Cavka, J. H.; Jakobsen, S.; Olsbye, U.; Guillou, N.; Lamberti, C.; Bordiga, S.; Lillerud, K. P. A New Zirconium Inorganic Building Brick Forming Metal Organic Frameworks with Exceptional Stability. *J. Am. Chem. Soc.* **2008**, *130*, 13850−13851.
(76) Guillerm, V.; Ragon, F.; Dan-Hardi, M.; Devic, T.; Vishnuvarthan, M.; Campo, B.; Vimont, A.; Clet, G.; Yang, Q.; Maurin, G.; et al. A Series of Isoreticular, Highly Stable, Porous Zirconium Oxide Based Metal−Organic Frameworks. *Angew. Chem., Int. Ed. Engl.* **2012**, *51*, 9267.
(77) Wiersum, A. D.; Soubeyrand-Lenoir, E.; Yang, Q.; Moulin, B.; Guillerm, V.; Ben Yahia, M.; Bourrelly, S.; Vimont, A.; Miller, S.; Vagner, C.; et al. An Evaluation of UiO-66 for Gas-Based Applications. *Chem. Asian J.* **2011**, *6*, 3270.
(78) Yang, Q.; Wiersum, A. D.; Llewellyn, P. L.; Guillerm, V.; Serre, C.; Maurin, G. Functionalizing Porous Zirconium Terephthalate UiO-66(Zr) for Natural Gas Upgrading: A Computational Exploration. *Chem. Commun.* **2011**, *47*, 9603.
(79) Jasuja, H.; Zang, J.; Sholl, D. S.; Walton, K. S. Rational Tuning of Water Vapor and CO2 Adsorption in Highly Stable Zr-Based MOFs. *J. Phys. Chem. C* **2012**, *116*, 23526−23532.
(80) Biswas, S.; van der Voort, P. A General Strategy for the Synthesis of Functionalised UiO-66 Frameworks: Characterisation, Stability and CO2 Adsorption Properties. *Eur. J. Inorg. Chem.* **2013**, 2154−2160.
(81) Granato, M. A.; Martins, V. D.; Ferreira, A. F. P.; Rodrigues, A. E. Adsorption of Xylene Isomers in MOF UiO-66 by Molecular Simulation. *Microporous Mesoporous Mater.* **2014**, *190*, 165−170.
(82) Ren, J. W.; Segakweng, T.; Langmi, H. W.; Musyoka, N. M.; North, B. C.; Mathe, M.; Bessarabov, D. Microwave-Assisted Modulated Synthesis of Zirconium-Based Metal-Organic Framework (Zr-MOF) for Hydrogen Storage Applications. *Int. J. Mater. Res.* **2014**, *105*, 516−519.
(83) Li, L. J.; Tang, S. F.; Wang, C.; Lv, X. X.; Jiang, M.; Wu, H. Z.; Zhao, X. B. High Gas Storage Capacities and Stepwise Adsorption in a UiO Type Metal-Organic Framework Incorporating Lewis Basic Bipyridyl Sites. *Chem. Commun.* **2014**, *50*, 2304−2307.
(84) Furukawa, H.; Gandara, F.; Zhang, Y. B.; Jiang, J. C.; Queen, W. L.; Hudson, M. R.; Yaghi, O. M. Water Adsorption in Porous Metal-Organic Frameworks and Related Materials. *J. Am. Chem. Soc.* **2014**, *136*, 4369−4381.
(85) Duerinck, T.; Denayer, J. F. M. Unusual Chain Length Dependent Adsorption of Linear and Branched Alkanes on UiO-66. *Adsorpt. Int. Adsorpt. Soc.* **2014**, *20*, 251−259.
(86) Bozbiyik, B.; Duerinck, T.; Lannoeye, J.; De Vos, D. E.; Baron, G. V.; Denayer, J. F. M. Adsorption and Separation of N-Hexane and Cyclohexane on the UiO-66 Metal-Organic Framework. *Microporous Mesoporous Mater.* **2014**, *183*, 143−149.
(87) Duerinck, T.; Bueno-Perez, R.; Vermoortele, F.; De Vos, D. E.; Calero, S.; Baron, G. V.; Denayer, J. F. M. Understanding Hydrocarbon Adsorption in the UiO-66 Metal-Organic Framework: Separation of (Un)saturated Linear, Branched, Cyclic Adsorbates, Including Stereoisomers. *J. Phys. Chem. C* **2013**, *117*, 12567−12578.
(88) Wu, H.; Chua, Y. S.; Krungleviciute, V.; Tyagi, M.; Chen, P.; Yildirim, T.; Zhou, W. Unusual and Highly Tunable Missing-Linker Defects in Zirconium Metal-Organic Framework UiO-66 and Their Important Effects on Gas Adsorption. *J. Am. Chem. Soc.* **2013**, *135*, 10525−10532.
(89) Lau, C. H.; Babarao, R.; Hill, M. R. A Route to Drastic Increase of CO2 Uptake in Zr Metal Organic Framework UiO-66. *Chem. Commun.* **2013**, *49*, 3634−3636.
(90) DeCoste, J. B.; Peterson, G. W.; Schindler, B. J.; Killops, K. L.; Browe, M. A.; Mahle, J. J. The Effect of Water Adsorption on the Structure of the Carboxylate Containing Metal-Organic Frameworks Cu-BTC, Mg-MOF-74, and UiO-66. *J. Mater. Chem. A* **2013**, *1*, 11922−11932.
(91) Cmarik, G. E.; Kim, M.; Cohen, S. M.; Walton, K. S. Tuning the Adsorption Properties of UiO-66 via Ligand Functionalization. *Langmuir* **2012**, *28*, 15606−15613.
(92) Barcia, P. S.; Guimaraes, D.; Mendes, P. A. P.; Silva, J. A. C.; Guillerm, V.; Chevreau, H.; Serre, C.; Rodrigues, A. E. Reverse Shape Selectivity in the Adsorption of Hexane and Xylene Isomers in MOF UiO-66. *Microporous Mesoporous Mater.* **2011**, *139*, 67−73.
(93) Ramsahye, N. A.; Trens, P.; Shepherd, C.; Gonzalez, P.; Khuong, T.; Ragon, F.; Serre, C. The Effect of Pore Shape on Hydrocarbon Selectivity on UiO-66 (Zr), HKUST-1 and MIL-125 (Ti) Metal Organic Frameworks: Insights from Molecular Simulations and Chromatography. *Microporous Mesoporous Mater.* **2014**, *189*, 222−231.
(94) Yang, Q.; Wiersum, A. D.; Guillerm, V.; Serre, C.; Llewellyn, P. L.; Maurin, G. Understanding the Thermodynamic and Kinetic Behavior of the CO 2/CH 4 Gas Mixture within the Porous Zirconium Terephthalate UiO-66 (Zr): A Joint Experimental and Modeling Approach. *J. Phys. Chem. C* **2011**, *115*, 13768−13774.
(95) Wu, D.; Maurin, G.; Yang, Q.; Serre, C.; Jobic, H.; Zhong, C. Computational Exploration of a Zr-Carboxylate Based Metal-Organic Framework as a Membrane Material for CO2 Capture. *J. Mater. Chem. A* **2014**, *2*, 1657−1661.
(96) Llewellyn, P. L.; Maurin, G. Gas Adsorption Microcalorimetry and Modelling to Characterise Zeolites and Related Materials. *C. R. Chim.* **2005**, 283−302.
(97) Llewellyn, P. L.; Maurin, G. Adsorption and Microcalorimetry on Molecular Sieves. In *Introduction to Zeolite Molecular Seives*; van Bekkum, H., Cejka, J., Corma, A., Schuth, F., Eds.; Elsevier: New York, 2007; pp 555−610.
(98) Yang, Q.; Zhong, C. Molecular Simulation of Carbon Dioxide/methane/hydrogen Mixture Adsorption in Metal-Organic Frameworks. *J. Phys. Chem. B* **2006**, *110*, 17776−17783.
(99) Rosenbach, N., Jr.; Ghoufi, A.; Deroche, I.; Llewellyn, P. L.; Devic, T.; Bourrelly, S.; Serre, C.; Ferey, G.; Maurin, G. Adsorption of Light Hydrocarbons in the Flexible MIL-53(Cr) and Rigid MIL-47(V) Metal−organic Frameworks: A Combination of Molecular Simulations and Microcalorimetry/gravimetry Measurements. *Phys. Chem. Chem. Phys.* **2010**, *12*, 6428−6437.
(100) Vlugt, T. J. H.; García-Pérez, E.; Dubbeldam, D.; Ban, S.; Calero, S. Computing the Heat of Adsorption Using Molecular Simulations: The Effect of Strong Coulombic Interactions. *J. Chem. Theory Comput.* **2008**, *4*, 1107.
(101) Smith, W.; Forester, T. R. DL _ POLY _ 2. 0: A General-Purpose Parallel Molecular Dynamics Simulation Package Overall Design. *J. Mol. Graph.* **1996**, *7855*, 136−141.
(102) Frenkel, D.; Smit, B. *Understanding Molecular Simulations: From Algorithms to Applications*, 2nd ed.; Academic Press: New York, 2001.
(103) Skoulidas, A. I.; Sholl, D. S. Transport Diffusivities of CH 4, CF 4, He, Ne, Ar, Xe, and SF 6 in Silicalite from Atomistic Simulations. *J. Phys. Chem. B* **2002**, *106*, 5058−5067.

(104) Martin, M. G.; Siepmann, J. I. Transferable Potentials for Phase Equilibria. 1. United-Atom Description of N -Alkanes. *J. Phys. Chem. B* **1998**, *102*, 2569−2577.
(105) Mayo, S. L.; Olafson, B. D.; Goddard, W. A., III DREIDING: A Generic Force Field for Molecular Simulations. *J. Phys. Chem.* **1990**, *94*, 8897−8909.
(106) Rappé, A. K.; Casewit, C. J.; Colwell, K. S.; Goddard, W. A., III; Skiff, W. M. UFF, a Full Periodic Table Force Field for Molecular Mechanics and Molecular Dynamics Simulations. *J. Am. Chem. Soc.* **1992**, *114*, 10024−10035.
(107) Lorentz, H. A. Ueber Die Anwendung Des Satzes Vom Virial in Der Kinetischen Theorie Der Gases. *Ann. Phys.* **1881**, *248*, 127−136.
(108) Berthelot, D. C. R. Sur Le Mélange Des Gaz. *Hebd. Seance. Acd. Paris* **1898**, *126*, 1703.
(109) Trung, T. K.; Déroche, I.; Rivera, A.; Yang, Q.; Yot, P.; Ramsahye, N.; Vinot, S. D.; Devic, T.; Horcajada, P.; Serre, C.; et al. Hydrocarbon Adsorption in the Isostructural Metal Organic Frameworks MIL-53(Cr) and MIL-47(V). *Microporous Mesoporous Mater.* **2011**, *140*, 114−119.
(110) Deroche, I.; Rives, S.; Trung Khuong, T.; Yang, Q.; Ghoufi, A.; Ramsahye, N. A.; Trens, P.; Fajula, F.; Devic, T.; Serre, C.; et al. Diffusion in the MOF-Type MIL-47 (V) Material by Combining Experimental and Molecular Simulation Tools. *J. Phys. Chem. C* **2011**, *115*, 13868−13876.
(111) Krishna, R.; van Baten, J. M. Loading Dependence of Self-Diffusivities of Gases in Zeolites. *Chem. Eng. Technol.* **2007**, *30*, 1235−1241.
(112) Heink, W.; Karger, J.; Pfeifer, H.; Datema, K. P.; Nowak, A. K. High-Temperature Pulsed Field Gradient Nuclear Magnetic Resonance Self-Diffusion Measurements of N-Alkanes in MFI-Type Zeolites. *J. Chem. Soc., Faraday. Trans.* **1992**, *88*, 3505−3509.
(113) Ford, D. C.; Dubbeldam, D.; Snurr, R. Q. The Effect of Framework Flexibility on Diffusion of Small Molecules in the Metal-Organic Framework IRMOF-1. *Diffus. Fundam.* **2009**, *11*, 1−8.
(114) Dubbeldam, D.; Beerdsen, E.; Calero, S.; Smit, B. Dynamically Corrected Transition State Theory Calculations of Self-Diffusion in Anisotropic Nanoporous Materials. *J. Phys. Chem. B* **2006**, *110*, 3164−3172.
(115) Combariza, A. F.; Sastre, G. Influence of Zeolite Surface in the Sorption of Methane from Molecular Dynamics. *J. Phys. Chem. C* **2011**, *115*, 13751−13758.